Impact of Boundary Layer Suction on Clearance Leakage Flow in a Cantilever Stator of Transonic Compressor

B. Zhang, B. Liu†, P. Liu and X. Mao

School of Power and Energy, Northwestern Polytechnical University, Xi'an, Shaanxi, 710072, P. R. China

†*Corresponding Author Email: liubo704@nwpu.edu.cn*

ABSTRACT

To control secondary flow effects and enhance the aerodynamic performance of the compressor, the flow control effects of the flow suction at the endwall with different circumferential positions and at the blade tip were numerically investigated in the cantilever stator of an axial single-stage transonic compressor. The main purpose was to gain a better understanding of the application of boundary layer suction and the associated control mechanisms in the cantilever stator. The studies show that the optimal position of the endwall suction slot should be located up the stator blade, in terms of the leakage flow structures and the blade tip unloading effect. In addition, the flow control effects of the suction at the blade tip on leakage flow upstream is better than that of the endwall flow suction with the same structure. Further, the studies of compressor aerodynamic performance curves illustrate that the efficiency and pressure ratio is increased by 0.34% and 1.09% at the peak efficiency point, and are increased by 0.39% and 0.14% at the near stall point, respectively.

Keywords: Tip leakage flow; Endwall suction; Blade tip suction; Suction flow rate; Active flow control.

NOMENCLATURE

ASTC	Axial Single-Stage Transonic Compressor		S_{ij}	strain-rate tensor
BLS	Boundary Layer suction		SFR	Suction Flow Rate
BTS	Blade Tip Suction		SS	Suction Surface
CS	Cantilever Stator		SV	Separation Vortex
ES	Endwall Suction		TE	Trailing Edge
h	height of stator		TLF	Tip Leakage Flow
Hn	Normalized Helicity		TLV	Tip Leakage Vortex
LE	Leading Edge		u_{ij}	components of a vector field
m	mass flow rate		W	relative flow velocity
NSP	Near Stall Point		y+	non-dimensional wall distance
PEP	Peak Efficiency Point			
PS	Pressure Surface		ω	absolute vorticity
PV	Passage Vortex		Ω_{ij}	spin tensor
Q	vortex determination criterion			

1. INTRODUCTION

Practically, there is a gap between the blade and the casing/hub to prevent the blade from touching the casing/hub. The flow near the gap generates the tip leakage flow (TLF) from the pressure surface (PS) of the blade to the suction surface (SS) under the pressure difference (Booth *et al.,* 1982; Inoue *et al.,* 1989). Generally, the leakage flow is mainly present in the form of the tip leakage vortex (TLV) because

of the influence of the endwall boundary layer and incoming main flow, and it has a great influence on the aerodynamic performance of the compressor due to the tip blockage. A research on the influence and control methods of TLF and TLV has been the matter of concern of scholars until now. A large number of studies showed that an appropriate clearance was beneficial to the compressor performance, which could control the corner separation (Shabbir *et al.,* 1997; Fischer *et al.,* 2011; Gottschall *et al.,* 2012).

But inappropriate clearance may result in enhancement of TLF, which makes the compressor efficiency decline and the stall margin reduce (Wheeler *et al.,* 2012; Zhong *et al.,* 2013; Chen *et al.,* 2013; Acharya *et al.,* 2013).

Kang and Hirsch (1994) measured the TLF in detail and studied the vortex structures in the endwall region. It was found that the tip vortices were composed of the leakage vortex, separation vortex and secondary vortex, which often referred to as the three vortex models.

As the emerging engine technology is developing towards high loading, there is still strong motivation to look for means to minimize the influence of TLF on the compressor performance. Therefore, there are numerous flow control methods being investigated to expand stall margin and improve compressor performance by altering the leakage vortex. The flow control methods are usually classified into active and passive categories. Generally, active flow control methods mainly include aspiration/suction techniques, tip injection (Taghavi-Zenouz *et al.,* 2018), plasma actuator (Akcayoz *et al.,* 2016) and acoustic excitation (Yarusevych *et al.,* 2005). The latter is mainly composed of sweep and dihedral (Copenhaver *et al.,* 1996; Benini *et al.,* 2007), casing treatment (Mao *et al.,* 2018a; 2018c), blade tip winglet (Zhong *et al.,* 2013; Jung *et al.,* 2018), vortex generators (Hergt *et al.,* 2012) and non-axisymmetric endwall (Liu *et al.,* 2017).

Several studies have been conducted to determine the effectiveness of BLS to improve compressor performance and to provide guidance during the design process of suction slots. Peacock *et al.* (1971) and Stratford's researches (1973) showed that BLS could effectively reduce the separation of the endwall and total pressure loss in the compressor. Meanwhile, Loughery *et al.* (1971) applied BLS to the stator vane of the compressor. It was found that suction on the surface of the compressor blade could significantly increase the capacity of the flow deflection and improve the efficiency, thereby significantly contributing towards improving the aerodynamic performance. Mao *et al.* (2018b) investigated three suction schemes located on the blade tip with different chordwise coverage. The results showed that the best scheme should be arranged at slightly downstream of the onset point of TLV. Similarly, there are some other studies to explore the influence of suction slot location and configuration on compressor performance (Leishman *et al.,* 2006a; 2006b; 2006c). Liesner *et al.* (2013) used two different setups with no recirculation or in-slot recirculation to determine the performance of BLS for secondary flow control. For the BLS, they stated that the velocity from passage to slot must be positive throughout the orifice to increase the compressor performance effectively. And some scholars have carried out the studies of BLS on the control of separated flow and TLF to improve compressor performance and stability (Dobrzynski *et al.,* Gümmer *et al.* and Gbadebo *et al.* 2008; Hubrich *et al.,* 2004; Jun *et al.* and Perry *et al.* 2017; Shi *et al.,* 2015; Zhao *et al.,* 2010, 2011). In addition, other study included the combination of

BLS and other flow control technologies (Ma *et al.,* 2018).The above researches showed that the BLS could effectively delay the separation of flow and decrease the loss, improving the performance of the compressor. In addition, that is also effective in controlling the TLF.

Most published literature are known to suck on the compressor blades, the casing of rotor and cascade endwall to modify the rotor flow field. By contrast, there is a lack of the experimental and numerical investigations about the endwall suction (ES) and blade tip suction (BTS) of a cantilever stator (CS). In this paper, the flow control effects of the ES with different circumferential positions and the BTS on the TLF were numerically investigated in the CS of an axial single-stage transonic compressor (ASTC). In order to control the TLF and modify the endwall flow field, as well as to uncover the associated control mechanisms, the focus of analysis in this paper will be mainly on: (1) studies were performed with respect to the ES and TS; (2) the tip flow field in CS was analyzed to gain an understanding of the flow changes and explain the study results. This paper is organized as follows. Firstly, the compressor stage and the numerical method were introduced in section 2.1 and 2.2. Then, the design of aspiration schemes is presented in section 2.3. The numerical results and discussion are presented subsequently in section 3, and finally, a list of conclusions is summarized in section 4.

2. INVESTIGATED COMPRESSOR STAGE AND THE NUMERICAL METHOD

2.1 Investigated Compressor Stage

A single-stage axial transonic compressor was used for the numerical investigation in this paper. The cross-sectional diagram of the compressor is shown in Fig. 1. Table 1 lists the main geometric and performance parameters of the compressor. In order to study TLF and TLV of cantilever stator, the gap size of the stator was set to 0.8mm.
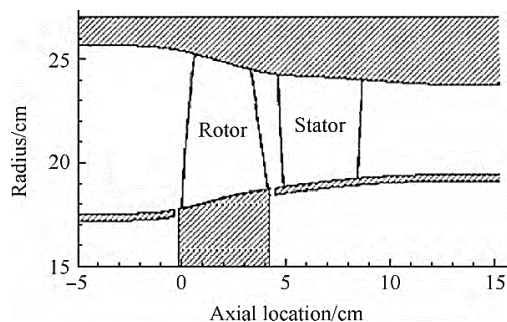
Fig. 1. Structure of the axial single-stage transonic compressor.

The main flow passage mesh was used AutoGrid5 from NUMECA International to generate a single-channel O4H mesh topology with a total grids number of approximately 1.85 million. The grid density was increased toward the solid boundaries to keep y+<9.3 at the walls with the minimum grid

spacing of $1 \times 10^{-6}m$ on the solid wall, which satisfied the applicable condition of the modeling of turbulence as shown in Fig. 2. In order to ensure the grid resolution and improve the accuracy of the calculation, 21 nodes used in the tip clearance region for the stator. Furthermore, the "butterfly grid" topology was used to ensure the grid quality in the gap. The computational mesh of compressor and local enlargement of mesh at the leading and trailing edges (LE, TE) of the stator blade tip is shown in Fig. 3.

Table 1 Design parameters of ASTC

parameters	values
Rotational speed（r/min）	-17188.7
Rotor blades count	36
Stator blades count	46
Rotor aspect ratio	1.19
Stator aspect ratio	1.26
Hub-tip radius ratio	0.7
Design tip speed（m/s）	454
Design pressure ratio	1.82
Design conversion flow（kg/s）	20.188
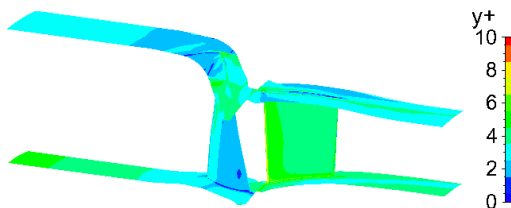
Fig. 2. Distribution of dimensionless wall distance.
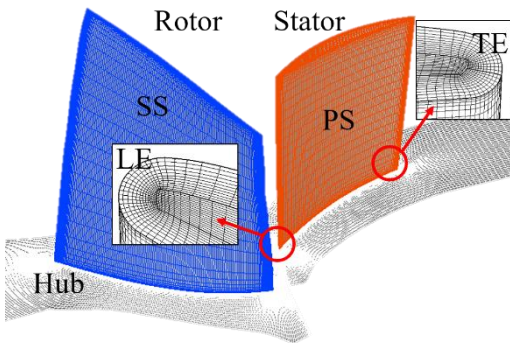
Fig. 3. Computational mesh of compressor and local enlargement of mesh at the stator blade tip.

2.2 Numerical Methodology and Validation

The numerical calculation was based on the steady simulation by using Fine/Turbo from NUMECA International to solve the Reynolds-averaged Navier-Stokes equations, and the working fluid selected the perfect gas. According to the literature of Glanville *et al.* (2001) and Lee *et al.* (2004), although the Spalart-Allmaras (S-A) turbulence model differs from the experimental values in the tip region, it agrees well in predicting the location, trajectory, and loss of TLV. Therefore, considering the calculation cost and robustness, the S-A turbulence model was

chosen as the turbulence model in this paper. A cell-centered finite volume scheme was chosen for the spatial discretization of equations. The time discretization was done using the explicit four-step Runge-Kutta scheme in the steady simulations. In addition, the CFL number was set to 3.0. At the inlet boundary conditions, the values of total parameters were applied, and the averaged static pressure was given as the outlet boundary condition. In addition, the mass of suction flow and the initial pressure were given as the outlet condition of the suction slot. Adiabatic and non-slip boundary conditions were applied on the sold walls.

In order to validate the calculation method adopted in the present work, the comparison between the numerical and experimental results was drawn by calculating the value of flow-turning angle of the rotor and stator at design speed with a mass flow rate of 20.13kg/s as shown in Fig. 4. The abbreviation "CFD" denotes the results of numerical simulation and "Exp" denotes the experimental results. The experimental data came from the NASA report (Reid *et al.,* 1978). The mass flow in the experiment was measured by a calibrated orifice flowmeter, and radial surveys of flow parameters were made using two combination probes and two wedge probes. The radial distribution of the flow angle involved in the figure was the result of the circumferential mass averaging. One can see that the trends of parameter distribution between the numerical and experimental results were mostly in a good agreement, especially the turning angle of the rotor. The flow turning angles of stator predicted by numerical simulations were slightly lower than the experimental value at the middle range and near the shroud, but this region did not represent the scope of this study. Therefore, the agreement between numerical simulation and experimental results gave us a reason to believe that the numerical method could be used to draw trustworthy conclusions about the flow features in the compressor.
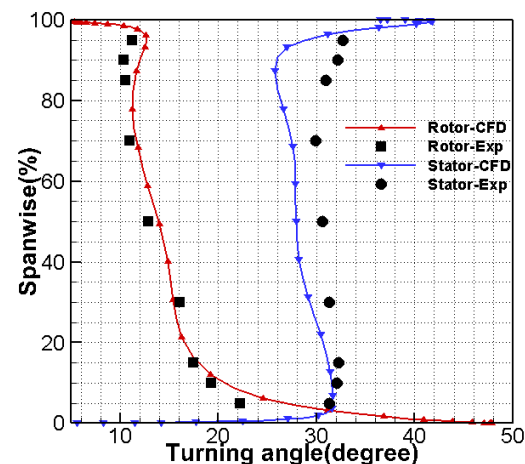
Fig. 4. Comparison of calculated and experimental flow turning angle at design speed with a mass flow of 20.13kg/s.

2.3 Design of Suction Slots

In order to explore the effect of BLS on the control

of TLV of the cantilever stator, we designed three schemes for ES with different circumferential positions, one BTS scheme and one ES scheme named EA that with the same slot geometry as the BTS scheme. The suction slots are used IGG from NUMECA International to generate an H-type topology with a node number of approximately 100,000. The slot mesh was connected with the mesh of blade passage by the full non-matching connecting technology that without significant numerical interpolation losses.

The slots of ES were curved along with the profile of the SS of the stator blade tip, and covered over the full axial chord length. Three schemes for the ES are shown as Fig. 5. The slot of scheme LA is located up the blade; that of the LB is close to the suction side; and the slot of LC is close to the pressure side of the blade.
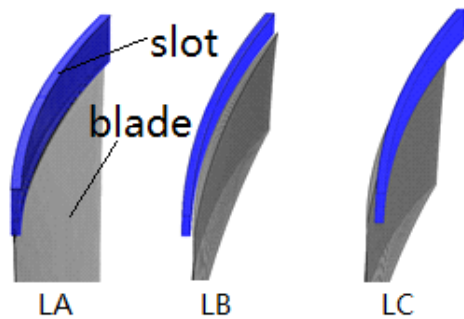
Fig. 5. Schematic diagram of schemes of ES.

The slot of BTS was curved along with the profiles of the SS and PS of the stator blade tip respectively, which adopted a wide middle and narrow ends structure. It covered over a position of 15% to 85% axial chord of the stator blade tip. The left diagram of Fig. 6 is the structure of the BTS scheme called TA. In order to compare the impacts between ES and BTS in controlling TLF and TLV, an ES scheme named EA that exactly as same as the slot geometry of BTS was calculated by numerical simulation. The structure of the EA scheme is shown on the right-hand side of Fig. 6. The two sides of the suction slot in this section were parallel to the blade tip camber at suction and pressure surfaces, which was different from the general suction slots of ES, so that the two ends of the slot were narrow while the middle part was wide.

3. RESULTS AND DISCUSSION

3.1 Research on the Endwall Suction Schemes

The LA scheme, as an example, was applied for suction within the flow margin, the suction flow rates (SFRs) were 0.5% and 1.0% of the inlet flow mass near stall operating condition respectively. The compressor aerodynamic performance curves are shown in Fig. 7. The overall distribution trends of the efficiency and pressure ratio almost unchanged whether suction or not, the efficiency

increased first and then decreased with the decrease of mass flow, the pressure ratio increased with the decrease of flow, while the growth rate became smaller and smaller. By comparing the curves, it was found that the efficiency and pressure ratio was increased after suction with the same mass flow. It was because that the slot absorbs the low-energy flow at the endwall, reduces the flow loss, and modifies the aerodynamic performance. The curves with suction in the whole flow range were above the original curve, and the increase of SFR of 1.0% is higher than that of 0.5%. The peak efficiency point (PEP) and the near stall point (NSP) were taken as examples. Figure 8 lists the change rates of performance parameters with and without suction in the LA scheme. The values in the figure depict that suction cannot only improve the performance of the compressor at the NSP, but also at other flow conditions, which proved the applicability of the suction over a large operating range. However, it had to be mentioned that the change in stall margin needed a further detailed discussion.
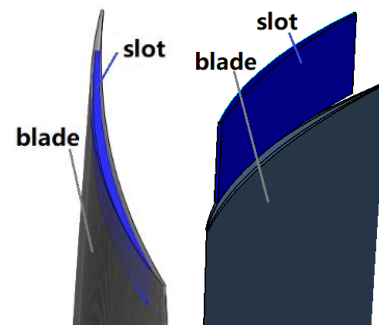
Fig. 6. Structure of scheme TA and EA.

In the previous paper, the LA scheme is taken as an example to illustrate the flow control effect of BLS on the overall performance of the compressor within the full flow margin. Next, we will select the NSP condition as a typical example to illustrate the flow control effect of each suction schemes on the TLF and TLV in the cantilever stator.

The results of the experiment published in 1991 by Storer and Cumpsty (1991) pointed that the minimum point of static pressure on the endwall coincided with the initial position of TLV, which moved downstream with the increase of the tip clearance size. Therefore, the minimum static pressure point on the endwall was used as the onset of TLV in this paper. Figure 9 shows the Q invariant and static pressure isolines of the stator passage near the endwall of the hub, it can be seen that the core of TLV extracted according to the Q criterion (Hunt *et al.,* 1988) coincides with the minimum static pressure groove on the end wall. In addition, according to the viewpoint of Inoue *et al.* (1989; 1998), it is considered that the motion trajectory of TLV corresponded to the curve on the static pressure inclined groove of the end wall in this paper.
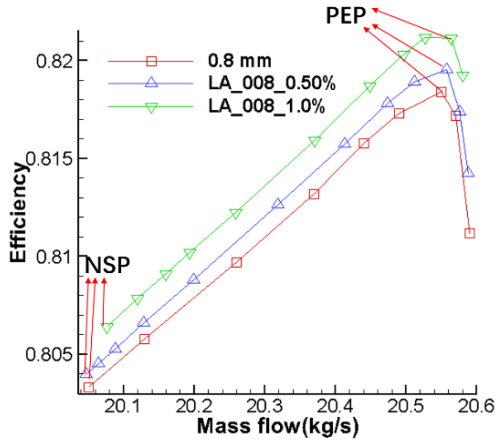
(a) Flow-efficiency
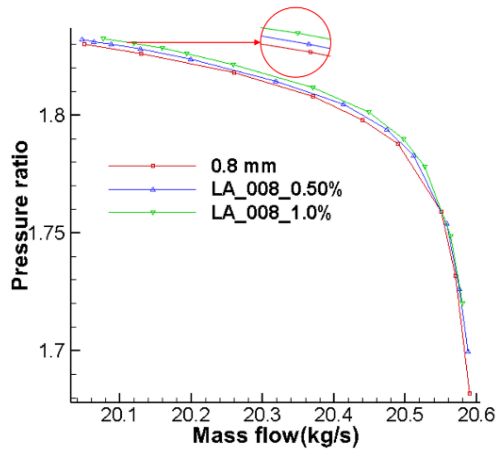
(b) Flow- pressure ratio

Fig. 7. Compressor aerodynamic performance.
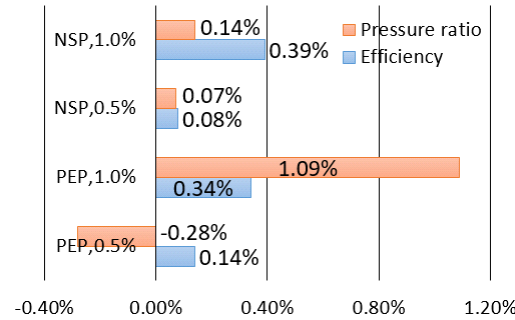
Fig. 8. The rates of change of efficiency and pressure ratio in the LA scheme.

Figure 10 shows the static pressure isolines at the stator hub endwall of each suction schemes of ES with different suction flow rates. The red curve added on each stator passage indicates the trajectories of TLV, which was connected by the minimum static pressure points. It is deduced from the diagram that the starting position of TLV was almost unchanged, but the path of TLV was gradually shifted toward the SS of the blade when the suction flow rate was small, indicating the weakness of TLV. The upstream change of the blade was less affected than that of the downstream, and the downstream of TLV was more offset to SS of the

stator blade. This phenomenon was caused by the smaller pressure difference between suction slot and endwall upstream, which resulted in smaller suction flow, while the pressure difference between the outlet of the suction slot and endwall downstream was larger which resulted in more suction flow. Therefore, suction had a greater influence on TLF of the upstream where the TLV started and fully developed than that of downstream where TLV mixed with the mainstream and dissipated gradually.
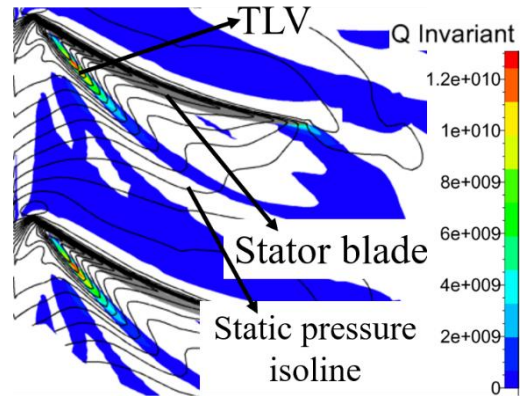
Fig. 9. Q Invariant and static pressure isolines of original stator passage.
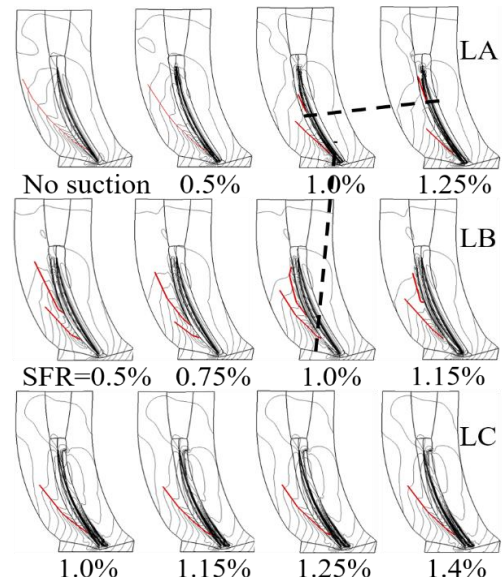
Fig. 10. Static pressure isolines of the endwall.

When the SFR was large, the trajectories of TLV were affected by the suction greatly. The initial positions of TLV changed a little, but then the connection curves of the minimum static pressure on endwall were greatly changed. Taking the LA scheme as an example with an SFR of 1%. The trajectory of TLV was divided into two sections instead of the one in common. The front curve was finally terminated at the position about 62% axial chord of stator blade tip due to the static pressure minimum channel widening gradually, which indicated that the TLV weakened gradually and

dissipated at the position. In addition, there was the other static pressure minimum channel on the downstream endwall, which depicted that the TLV was enhanced gradually at the middle channel after the brief disappearance. As well as it could be visible from the three-dimensional streamlines at clearance on the mid-gap. The streamlines of leakage flow were straight in the middle after the bent at the blade LE, which showed that the intensity and scale of TLV decreased obviously since the velocity of TLF was closer to that of the main flow. Comparing and analyzing the length of the trajectory of TLV and the distance that TLV from the blade SS of the three ES schemes, it could be tentatively drawn the conclusion that the LA scheme was the best of the three schemes in controlling TLF and TLV. I.e. the optimal position of the ES slot should be located up the stator blade.

The three-dimensional streamlines of TLF under the same suction flow rate for each ES schemes are shown in Fig. 11. It can be seen from the figure that the TLF with suction was obviously weakened, but the effects of flow controlling were also different as the slots have different circumferential positions relative to the stator blade. The flow at the middle chord position relative to the blade was basically sucked out with suction of the LA scheme. Only some leakages existed near the blade LE and TE. The LB scheme has more number of streamlines than the LA scheme, that is, the control effect was worse than that of the LA scheme with the same SFR. The LC scheme retained the most number of streamlines, which means the worst control effect on the TLF. That was the same as the conclusion obtained from the analysis of the static pressure contour on the hub endwall.
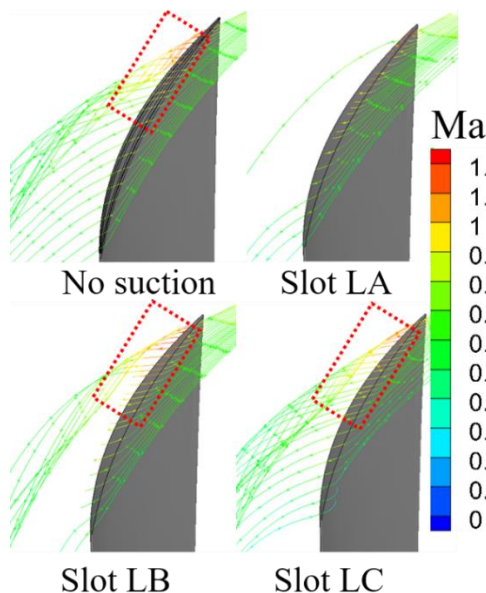
pressure loss was inaccurate in the detailed simulation of the hub leakage flow, while the calculation of the entropy increase on the stator was a better measure of relative performance. Therefore, efficiency and entropy were used to measure the flow field while describing and analyzing the TLF and flow suction effect. In order to explore the reason for the difference of flow control effects among the three suction schemes of ES, the surface streamlines and entropy contour on slice normal to the axial direction at 35% axial chord of blade tip under an SFR of 1.0% are presented in Fig. 12. The vortex near the stator blade SS was the structure of the TLV, and the other at the gap inlet was the separation vortex (SV). Through the comparison of the conditions with and without suction, it was found that the region of TLV decreased and of SV increased. With the LA scheme, the TLV structure was almost invisible, indicating a good effect of suction on controlling the TLF. The area of TLV with the LB scheme was significantly greater than that of the LA scheme. Although the area of the TLV with the LC scheme was slightly smaller than that with the LB scheme, the position of the vortex core was farther away from the blade SS, and the high-entropy region was larger. It is because of the fact that the TLF was generated from the pressure side to the suction side of the blade resulting in TLV. When the pressure side was slotted and sucked, the flow has better aerodynamic performance because it had not been accelerated by the gap. The suction near the suction side had been separated from the pressure side and led to the lower energy. The suction up the stator blade can not only absorb some part of the flow that participated in the leakage vortex, but also some part of the separation flow. Therefore, it is the reason why the flow control effect of the scheme that slot up the stator blade is the best.

Fig. 11. Three-dimensional streamlines of TLV with SFR of 1.0%.
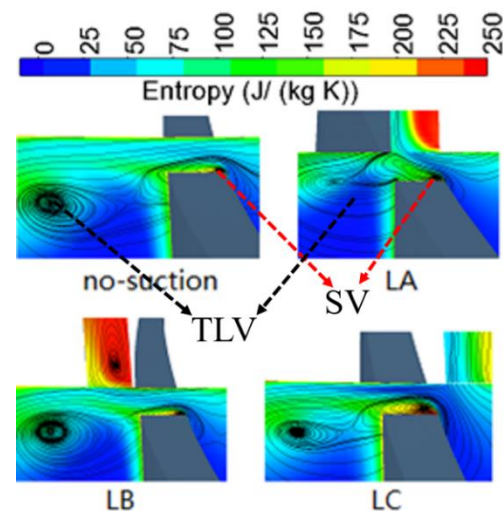
Fig. 12. Streamlines/entropy contour on 35% axial chord slices with SFR of 1.0%.

Sungho *et al.* (2015) studied an article regarding how to measure and evaluate the overall performance and the local flow field of the compressor. It emphasized that the traditional loss coefficient considering only

Figure 13 shows the normalized helicity H_n on different axial slices of the ES schemes with an SFR of 1.0%. The normalized helicity is defined as follows:

$$H_n = \frac{\overline{W} \cdot \overline{\omega}}{|\overline{W}| \cdot |\overline{\omega}|} \qquad (1)$$

where $\overline{W}$ and $\overline{\omega}$ denote vectors of the relative flow velocity and the absolute vorticity, respectively. The normalized helicity, which is the cosine of the angle between the velocity and vorticity vectors, reach its highest absolute numbers in the vortex-core regions. That could be used to locate the vortex axis (Degani *et al.,* 1990; Yamada *et al.,* 2008). The part near SS of the blade with the value of H_n approaching 1 on each slices was the core region of TLV, which was connected by a black dotted arrow to represent the trajectory of the TLV. The high H_n region near the PS of the adjacent blade was the passage vortex (PV). We can see from the figure that the TLV began near the LE of the blade, and its strength and influence range gradually increased and expanded as it developed downstream. Comparing with the normalized helicity distribution, BLS on endwall reduced the high value area and made the core of TLV close to the blade SS. The influence range and strength of TLV decreased, especially, the TLV of the scheme LA was almost invisible. According to the trajectory of TLV and the high value area of H_n marked by the black wire frame on the slice near the blade TE, the LA scheme had the best flow control effect on the TLV among the three schemes, while the LC scheme had the least obvious effect. Since the PV and TLV had a long-term relationship (Beselt *et al.,* 2014), the above conclusions could be indirectly proved by comparing the development trajectory and range of influence of the PV.
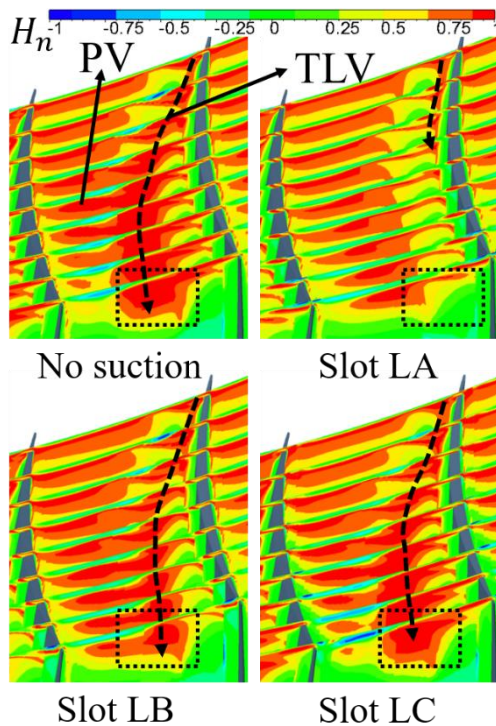
Fig. 13. The normalized helicity on different axial slices of ES with SFR of 1.0%.

In order to reflect the position and size changes of the

vortices visually, Fig. 14 shows the contour of the three-dimensional vortices given according to the Q criterion of determining of the vortices. The isosurface in the figure is $Q = 5 \times 10^6$. In this paper, Q was defined as:

$$Q = \frac{1}{2}\left(\Omega_{ij}\Omega_{ij} - S_{ij}S_{ij}\right) \qquad (2)$$

where $\Omega_{ij} = (u_{ij} - u_{ji})/2$ and $S_{ij} = (u_{ij} + u_{ji})/2$ are the spin tensor and strain-rate tensor, respectively. From the observation of Fig. 14, it can be seen that the three-dimensional vortex structures in the end-wall passage of the cantilever stator were consistent with the development of TLV studied in the previous studies, such as streamlines, entropy and normalized helicity. In the figure, the structures of TLV were labelled by the arrows and shown by the red dotted lines. The TLV resulted in blockage of flow passages and flow loss. The structures of TLV could be changed and the blocking effect could be weakened by suction on the endwall. The LA scheme had the most obvious weakening of the vortex structures among the three ES schemes, the TLV in adjacent passages could not be visible at the same view, which indicated that the TLV were obviously suppressed and the flow field near the gap was modified, thus improving the compressor performance.
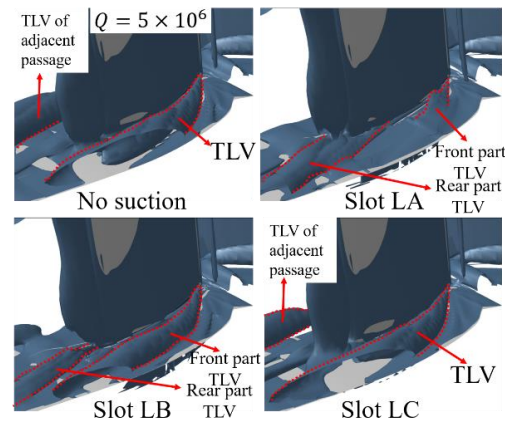
Fig. 14. Q-Isosurface of ES.

The static pressure distributions on 5% relative blade height of the ES are shown in Fig. 15 to quantify and compare the flow control effects. It is worth mentioning that all the statements about relative blade height in this paper refer to the hub plane as the benchmark, but the blade tip refers to the gap end near the hub. The trends of the static pressure distribution of the 5% blade span of every ES schemes were similar to that of no suction, whereas the static pressure changed in various degree. The main change of the LA scheme was the increase of the pressure on the blade SS due to the weakening of the TLF and the accumulation of the low energy fluid on the side of the blade SS, which thus reduced the flow velocity and increased the static pressure of the fluid. The static pressure on the blade SS of the LB scheme decreased upstream and increased downstream, which was different from the pressure

change whether or not suction in the LA scheme. The reason for this phenomenon was that the suction closed to the blade SS weakened the blockage effect of the low-energy fluid lead to the flow rate increased near the blade/endwall junction, and then the static pressure decreased because of the increase of flow velocity. Both of the two schemes have little changes on the static pressure of the stator blade PS. However, the main change of the LC scheme was the static pressure of the blade PS. The static pressure at the stator blade LE decreased after suction, but that started to increase from the middle chord. The decrease in the pressure was caused by the decrease of the blade tip loading due to suction. The possible reason for the increase of the pressure from the middle chord was that the tangential velocity of the flow near the blade tip was changed by suction. That is, the pressure increases as the decrease of the circumferential velocity of TLF. According to the distribution of the circumferential mass average entropy of the stator exit along with the relative blade height in Fig. 16, the entropy of the suction schemes had the same radial distribution trends. It is illustrated that the loss in the middle-span and near gap was lower with suction, especially in the range of 5% to 35% relative blade height. We can see that the three suction schemes could reduce the entropy overall the blade height range, which indicated that the ES could reduce the stator channel loss of the compressor by the aspiration of TLF and TLV. The average entropy distribution at stage outlet of the LA and LB schemes was the same, however, that of the LC scheme was obviously different from the former two schemes below 35% relative blade height. Entropy increased in the range of 5%-35% relative blade height, and less in the area below 5%. The LC scheme had the lowest overall entropy reduction, which meant that the scheme had the worst flow suction effect.
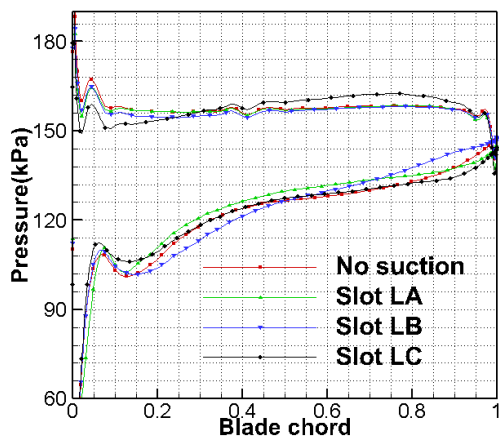
Fig. 15. Static pressure distribution of 5% span in the stator blade.

According to the analysis above, it can be concluded that ES could effectively weaken the TLF and TLV, and the flow suction effect gradually became more significant with the increase of the SFR. The optimal position of the slot for ES should be located up the stator blade in terms of TLF structures and the blade tip unloading effect at the near stall condition. And that slot located near the blade PS is the worst.
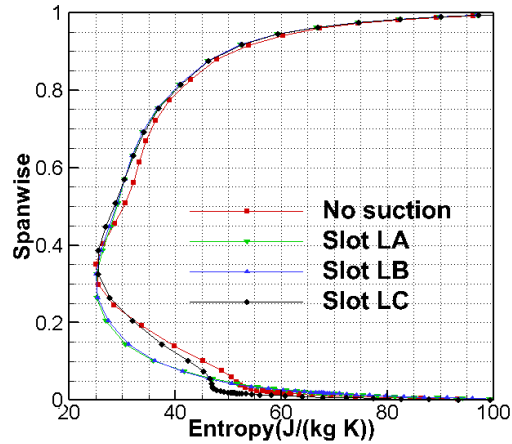
Fig. 16. Circumferential average entropy distribution of the stator exit.

3.2 Research on the Blade Tip Suction Scheme

The static pressure isolines of the endwall near the hub of the TS scheme (TA) and ES scheme (EA) are shown in Fig. 17, in which the red curves represent the TLV motion tracks. The TLV at the blade LE of the two suction schemes was reduced to some extent, but the decrease of that was obviously weakened compared with the previous full-chord slot schemes of the ES. The cause of this phenomenon was that the slot of the EA and TA schemes were both downstream of the starting point of TLV, which did not inhibit the formation of TLV. These two cases only reduced the fluid converging to the TLV in the mid-axial chord part, the two schemes only weaken the development process of TLV. Furthermore, there was a new leakage vortex trajectory started near the TE of the blade called rear part TLV, and the corresponding influence range was small, finally, merged with the leakage vortices of the front part. Compared with the two schemes, the TLV core line starting near the blade LE of the TS scheme was shorter and closer to the blade SS with the same SFR, while the intensity of TLV starting near the blade TE of the EA scheme was weaker than that of the TS scheme. Next, this section took the SFR of 0.5% as an example to illustrate the flow control effects of BTS and ES on the TLF in the CS. Through the three-dimensional streamlines of TLF in Fig. 18, after the suction with the TA and EA schemes, the streamlines originally located in the middle position were removed, which weaken the strength of TLV in the front end. This part TLF greatly reducing the range of influence of the TLV, and eventually integrates with the leakage flow originating near the blade TE. One can be clearly seen that the winding structure of TLV near the blade LE of the TA scheme was weaker than that of the EA, while that near the blade TE was stronger. It seemed to indicate that the BTS had a strong control effect on TLF near the blade LE, but the control of TLF near the blade TE was weak.

Figure 19 shows the flow streamlines and entropy contour of the axial slice at the 40% axial chord of the stator blade tip with an SFR of 0.5%. It can be found that the influence area of the TLV of this slice

was decreased with the suction of the two schemes, which indicated that the two schemes could effectively weaken the TLV strength. What is echoed with the analysis above is that the TLV of the TA scheme was obviously weaker than that of the EA scheme? The possible reason is that the TA scheme started to suck from the 15% chord position, and the EA scheme was the same, but the flow removed by the TA scheme was closer to the stator blade rather than to the endwall. The specific and deeper reasons would be analyzed in the following part.
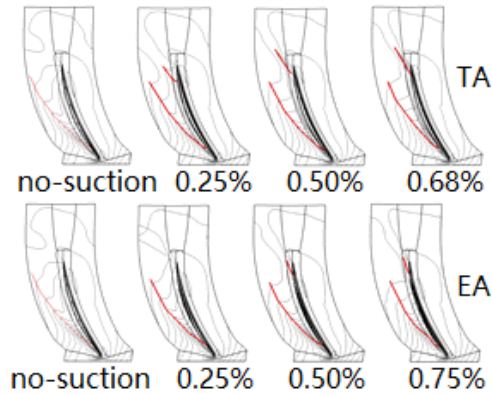
Fig. 17. Static pressure contour distribution on the end wall of the stator hub.
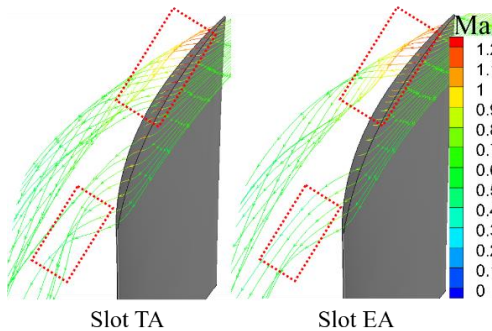
Fig. 18. 3D streamlines of the TLF with an SFR of 0.5%.

The normalized helicity on different axial slices of the TA and EA schemes with an SFR of 0.5% is shown on Fig. 20. Wherever the numerical value is higher, the vortex core region is represented. The TLV was near the stator blade SS, and its development trajectories were marked with the black dotted arrows in the figure. The PV was near the PS of the adjacent blade. During the development of the vortex from upstream to downstream of the stator passage, the influence range of TLV gradually increased, and the core gradually moved away from the blade SS, while the PV gradually weakened. Compared with the condition without suction in Fig. 13, the scheme TA and EA weakened the influence range of TLV and made the core region of TLV close to the blade SS slightly. The initial stages of TLV development of both schemes had no obvious difference. Comparing the ranges surrounded by the black wireframes on the last slice near the blade TE, the high-value area of the TA scheme was larger than

that of the EA. From the information reflected in this figure, one can notice that the EA scheme was better than the TA scheme in controlling the TLV near the stator blade TE, which could also be obtained from the three-dimensional leakage streamlines diagram. Similarly, as analyzed in Fig. 13, the above conclusions ccould also be cited laterally by comparing the development of PV and its influence range.
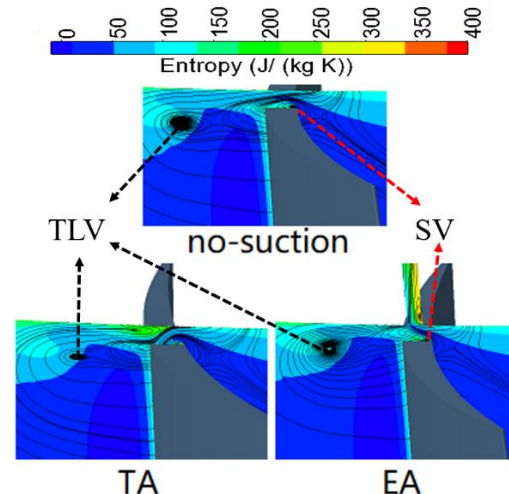
Fig. 19. Streamlines/entropy contour on 40% chord slices with SFR of 0.5%.
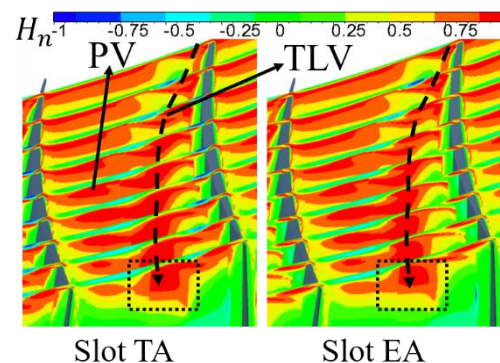
Fig. 20. The normalized helicity on different axial slices of TS with SFR of 0.5%.

Figure 21 shows the isosurface of the three-dimensional vortex structures of the two schemes given according to the Q criterion of determining of the vortices. The structures of TLV reflected in the figure are in accordance with the variation law of TLV analyzed above. Compared with the two schemes, the size of the rear part TLV in the TA scheme was larger than that in the EA scheme, while the size of the front part TLV was slightly smaller. This was mutually confirmed with the analysis results of the Figs. 18, 19 and 20.

The static pressure distributions of 5% relative blade height with an SFR of 0.50% are shown in Fig. 22. According to that, the static pressure on the PS of the stator blade decreased to a small extent from the starting position of the suction slot.

Static pressure on the blade SS at upstream of the TS scheme was greater than that of the ES scheme, and the downstream part was opposite. The reason for this was that the vorticity of TLV at the upstream and the radial influence range were large, while that of the downstream were small because of the mixing of the mainstream and the secondary flow. The blade tip suction could absorb the TLV with a strong winding structure at the upstream and only absorb the TLF that gently developed at the downstream. Therefore, the BTS had a more significant effect on controlling the TLV at the upstream. According to literature (Mao *et al.,* 2018c; Du *et al.,* 2013), this part of the TLF called main TLF was usually released from the blade LE to about 30% blade chord.
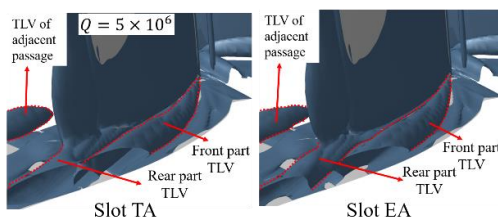
Fig. 21. Q-Isosurface of BTS.
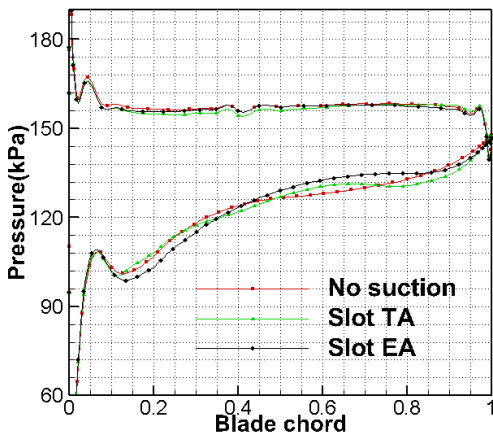
Fig. 22. Static pressure distribution of 5% span.
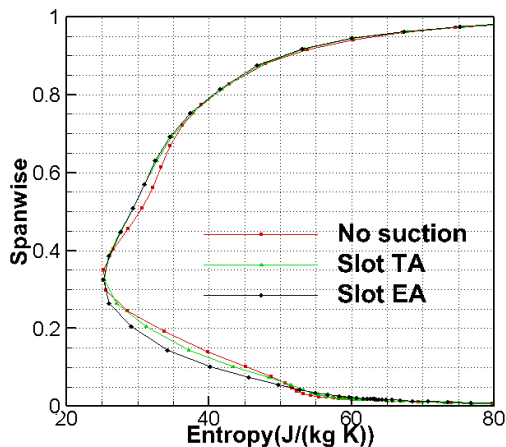
Fig. 23. The entropy distribution at stator outlet.

The entropy distributions of circumferential mass average at the stator outlet with the SFR of 0.5% are given as Fig. 23. As can be seen from the figure, compared with the operation without suction, the entropy obtained after suction was significantly changed in the middle blade height part and the region near the gap. The entropy of the two suction schemes was lower than that of the original condition in the range of 40%-75% relative blade height, and there was no difference between the two schemes. This was the result of redistribution of loading along the radial direction. The entropy of both schemes was also lower than that of the non-suction scheme in the range below 35% relative blade height, but the entropy of the EA scheme was much smaller, which indicated that the EA scheme was more conducive to modifying the flow field in the region near the endwall. This corroborated that the previous analysis that the EA scheme had a better flow control effect on downstream leakage flow.

In this section, the influence of the BTS and ES on the TLF was studied. According to the analysis of the flow streamlines, the static pressure on the endwall and the distribution of aerodynamic parameters on the outlet, we could conclude that the BTS with the same geometries of suction slots of the ES could reduce the TLF. However, the main influence of the chordwise position was different from the schemes of endwall suction, and a better flow control effect on the upstream leakage flow was obtained.

4. CONCLUSION

The application of the ES and BTS on the cantilever stator of an axial single-stage transonic compressor has been numerically investigated. The flow control effect of the BLS on the TLF behaviors inside and the corresponding flow control mechanisms of the endwall performance improvement have been carefully analyzed. The conclusions can be drawn as follows.

(1) The clearance flow field can be modified and the leakage vortex can be weakened by suction on the endwall of stator hub. For the same suction slot, the intensity and influence range of TLV decreases with the increase of the SFR. The rear part of the leakage vortex trajectory is more affected by suction than the former. In the case of the same SFR, the optimal position of the endwall suction slot should be located up the stator blade in terms of the leakage flow structures and the blade tip unloading effect at the near stall condition. In addition, the worst position is near the blade PS among the three schemes designed in this paper.

(2) The overall performance of the compressor can be obviously enhanced by the proper suction scheme on the blade tip of the cantilever stator. Moreover, the damage of TLV to the flow field in the endwall region is weakened. Similar to the endwall suction, the TLF and TLV are

more effectively controlled with the increase of the SFR. Compared with the flow suction on the endwall with the same SFR, the leakage vortex near the LE of the blade tip is closer to the blade SS, which has a more obvious inhibitory effect to the TLF near the blade LE and reduces the blocking effect of the passage largely.

(3) From the section of static pressure distribution, it can be seen that with suction, the blade load redistributes along the blade tip chord direction, and the change corresponds to the strength and structure change of TLV.

(4) Both the ES and BTS can reduce the TLF and TLV under different flow conditions, and with the increase of SFR, the degree of weakening effect to the TLF gradually increases. The extra loss caused by suction slot cannot be neglected in practical application. The reasonable suction scheme and the structure of the suction slot are of great significance to the design of the compressor in the future. Besides, as an active control technology requiring additional energy consumption, its impact of the BLS technology on stall margin and combination benefits are the focus of further study on the application of the suction technology in compressors.

ACKNOWLEDGMENTS

REFERENCES

Acharya, S., and L. Moreaux (2013). Numerical Study of the Flow Past a Turbine Blade Tip: Effect of Relative Motion Between Blade and Shroud. *Journal of Turbomachinery* 136(3), 031015.

Akcayoz, E., H. D. Vo and A. Mahallati (2016). Controlling Corner Stall Separation with Plasma Actuators in a Compressor Cascade. *Journal of Turbomachinery* 138(8), 081008.

Benini, E. and R. Biollo (2007). Aerodynamics of swept and leaned transonic compressor-rotors. *Applied Energy* 84(10), 1012-1027.

Beselt, C., M. Eck and D. Peitsch (2014). Three-Dimensional Flow Field in Highly Loaded Compressor Cascade. *Journal of Turbomachinery* 136(10), 101007.

Booth, T. C., P. R. Dodge and H. K. Hepworth (1982). Rotor-Tip Leakage: Part I–Basic Methodology. *Journal of Engineering for Power* 104(1), 154-159.

Chen, S., S. Sun, Y. Lan and S. Wang (2013). The effect of different clearance geometry configurations on aerodynamic performance in a high-load compressor cascade. *Proceedings of the Institution of Mechanical Engineers, Part G: Journal of Aerospace Engineering* 228(8), 1425-1433.

Copenhaver, W. W., E. R. Mayhew, C. Hah and A. R. Wadia (1996). The Effect of Tip Clearance on a Swept Transonic Compressor Rotor. *Journal of Turbomachinery* 118(2), 230-239.

Degani, D., A. Seginer and Y. Levy (1990). Graphical visualization of vortical flows by means of helicity. *AIAA Journal* 28(8), 1347-1352.

Dobrzynski, B., H. Saathoff, G. Kosyna, C. Clemen and V. Gümmer (2008). Active Flow Control in a Single-Stage Axial Compressor Using Tip Injection and Endwall Boundary Layer Removal. *ASME Turbo Expo: Power for Land, Sea, and Air* 6, 139-148.

Du, J., F. Lin, J. Chen, C. Nie and C. Biela (2013). Flow Structures in the Tip Region for a Transonic Compressor Rotor. *Journal of Turbomachinery* 135(3), 031012.

Fischer, A., L. Büttner, J. r. Czarske, M. Gottschall, R. Mailach and K. Vogeler (2011). Investigation of the Tip Clearance Flow in a Compressor Cascade Using a Novel Laser Measurement Technique with High Temporal Resolution. *ASME Turbo Expo: Turbine Technical Conference and Exposition* 7, 13-23.

Gbadebo, S. A., N. A. Cumpsty and T. P. Hynes (2007). Control of Three-Dimensional Separations in Axial Compressors by Tailored Boundary Layer Suction. *Journal of Turbomachinery* 130(1), 011004.

Glanville, J. P. (2001). Investigation into Core Compressor Tip Leakage Modelling Techniques Using a 3D Viscous Solver. *ASME Turbo Expo: Power for Land, Sea, and Air* 1, V001T03A035.

Gottschall, M., R. Mailach and K. Vogeler (2012). Penny Gap Effect on Performance and Secondary Flowfield in a Compressor Cascade. *Journal of Propulsion and Power* 28(5), 927-935.

Gümmer, V., M. Goller and M. Swoboda (2008). Numerical Investigation of End Wall Boundary Layer Removal on Highly Loaded Axial Compressor Blade Rows. *Journal of Turbomachinery* 130(1), 011015.

Hergt, A., R. Meyer and K. Engel (2012). Effects of Vortex Generator Application on the Performance of a Compressor Cascade. *Journal of Turbomachinery* 135(2), 021026.

Hubrich, K., A. Bölcs and P. Ott (2004). Boundary Layer Suction via a Slot in a Transonic Compressor: Numerical Parameter Study and First Experiments. *ASME Turbo Expo: Power*

for Land, Sea, and Air 5, 527-536.

Hunt, J. C. R., A. Wray and P. Moin (1988). Eddies, streams, and convergence zones in turbulent flows. *NASA N89*-24555, 18-34.

Inoue, M. and M. Kuroumaru (1989). Structure of Tip Clearance Flow in an Isolated Axial Compressor Rotor. *Journal of Turbomachinery* 111(3), 250-256.

Inoue, M., M. Furukawa, K. Saiki and K. Yamada (1998). Physical Explanations of Tip Leakage Flow Field in an Axial Compressor Rotor. *ASME International Gas Turbine and Aeroengine Congress and Exhibition 1, V001T01A027*.

Jun, D., D. Xin, C. Shaowen, Z. Xun, W. Songtao and S. Jiaqi (2017). Influence of Tailored Boundary Layer Suction on Aerodynamic Performance in Bowed Compressor Cascades. *ASME Turbo Expo: Turbomachinery Technical Conference and Exposition* 2A, V02AT39A004.

Jung, J. H. and W. G. Joo (2018). Effect of tip clearance, winglets, and shroud height on the tip leakage in axial flow fans. *International Journal of Refrigeration* 93, 195-204.

Kang, S. and C. Hirsch (1994). Tip Leakage Flow in Linear Compressor Cascade. *Journal of Turbomachinery* 116(4), 657-664.

Lee, G. H., J. I. Park and J. H. Baek (2004). Performance Assessment of Turbulence Models for the Quantitative Prediction of Tip Leakage Flow in Turbomachines. *ASME Turbo Expo: Power for Land, Sea, and Air* 5, 1501-1512.

Leishman, B. A., and N. A. Cumpsty (2006a). Mechanism of the Interaction of a Ramped Bleed Slot with the Primary Flow. *Journal of Turbomachinery* 129(4), 669-678.

Leishman, B. A., N. A. Cumpsty and J. D. Denton (2006b). Effects of Bleed Rate and Endwall Location on the Aerodynamic Behavior of a Circular Hole Bleed Off-Take. *Journal of Turbomachinery* 129(4), 645-658.

Leishman, B. A., N. A. Cumpsty and J. D. Denton (2006c). Effects of Inlet Ramp Surfaces on the Aerodynamic Behavior of Bleed Hole and Bleed Slot Off-Take Configurations. *Journal of Turbomachinery* 129(4), 659-668.

Liesner, K., R. Meyer, C. Gmelin and F. Thiele (2013). On the Performance of Boundary Layer Suction for Secondary Flow Control in a High Speed Compressor Cascade. *43rd Fluid Dynamics Conference*, San Diego, CA, AIAA paper 2013-2749.

Liu, X., D. Jin and X. Gui (2017). Investigation of non-axisymmetric endwall contouring in a compressor cascade. *Journal of Thermal Science* 26(6), 490-504.

Loughery, R. J., R. A. Horn and P. C. Tramm (1971). Single stage experimental evaluation of boundary layer blowing and bleed techniques for high lift stator blades. *NASA-CR-54573.*.

Ma, S., W. Chu, H. Zhang and C. Liu (2018). Impact of a Combination of Micro-Vortex Generator and Boundary Layer Suction on Performance in a High-Load Compressor Cascade. *ASME Turbo Expo: Turbomachinery Technical Conference and Exposition* 2A, V02AT39A011.

Mao, X., B. Liu and H. Zhao (2018a). Numerical analysis of the circumferential grooves casing treatment in a counter-rotating axial flow compressor. *Applied Thermal Engineering* 130, 29-39.

Mao, X., B. Liu and T. Tang (2018b). Control of Tip Leakage Flow in Axial Flow Compressor Cascade by Suction on the Blade Tip. *Journal of Applied Fluid Mechanics* 11(1), 137-149.

Mao, X., B. Liu, T. Tang and H. Zhao (2018c). The impact of casing groove location on the flow instability in a counter-rotating axial flow compressor. *Aerospace Science and Technology* 76, 250-259.

Peacock, R. E. (1971).*Boundary-layer Suction to Eliminate Corner Separation in Cascades of Aerofoils*. Ph.D. thesis, HM Stationery Office.

Perry, A. T. and P. J. Ansell (2017). Crossflow Fan Power Requirements for Boundary-Layer Suction in Transonic Flow. *Journal of Aircraft* 54(3), 1217-1220.

Reid, L., and R. D. Moore (1978). Performance of a Single- Stage Axial-Flow Transonic Compressor with Rotor and Stator Aspect Ratios of 1.19 and 1.26, Respectively, and with Design Pressure Ratio of 1.82. *NASA TP-1338*.

Shabbir, A., M. L. Celestina, J. J. Adamczyk and A. J. Strazisar (1997). The Effect of Hub Leakage Flow on Two High Speed Axial Flow Compressor Rotors. *ASME International Gas Turbine and Aeroengine Congress and Exhibition* 1, V001T03A053.

Shi, L., B. Liu, Z. Na, X. Wu and X. Lu (2015). Experimental investigation of a counter-rotating compressor with boundary layer suction. *Chinese Journal of Aeronautics* 28(4), 1044-1054.

Storer, J. A., and N. A. Cumpsty (1991). Tip Leakage Flow in Axial Compressors. *Journal of Turbomachinery* 113(2), 252-259.

Stratford, B. S. (1973). The Prevention of Separation and Flow Reversal in the Corners of Compressor Blade Cascade. *The Aeronautical Journal* 77(749), 249-256.

Sungho, Y., S. Rudolf, C. Patricia and W. Peter (2015). Effect of the Stator Hub Configuration and Stage Design Parameters on Aerodynamic Loss in Axial Compressors. *Journal of Turbomachinery* 137(9),091001.

Taghavi-Zenouz, R., and M. H. Ababaf Behbahani

(2018). Improvement of aerodynamic performance of a low speed axial compressor rotor blade row through air injection. *Aerospace Science and Technology* 72, 409-417.

Wheeler, A. P. S., T. Korakianitis and S. Banneheke (2012). Tip-Leakage Losses in Subsonic and Transonic Blade Rows. *Journal of Turbomachinery* 135(1), 011029.

Yamada, K., K. Funazaki and H. Sasaki (2008). Numerical Investigation of Relation between Unsteady Behavior of Tip Leakage Vortex and Rotating Disturbance in a Transonic Axial Compressor Rotor. *ASME Turbo Expo: Power for Land, Sea, and Air* 6, 425-436.

Yarusevych, S., J. G. Kawall and P. E. Sullivan (2005). Airfoil Performance at Low Reynolds Numbers in the Presence of Periodic Disturbances. *Journal of Fluids Engineering* 128(3), 587-595.

Zhao, B., S. Li, Q. Li and S. Zhou (2010). Unsteady Numerical Research Into the Impact of Bleeding on Axial Compressor Performance. *ASME 3rd Joint US-European Fluids Engineering Summer Meeting collocated with 8th International Conference on Nanochannels, Microchannels, and Minichannels* 1, 531-538.

Zhao, B., S. Li, Q. Li and S. Zhou (2011). The Impact of Bleeding on Compressor Stator Corner Separation. *ASME-JSME-KSME Joint Fluids Engineering Conference* 1, 531-537.

Zhong, J., S., Han, H. Lu and X. Kan (2013). Effect of tip geometry and tip clearance on aerodynamic performance of a linear compressor cascade. *Chinese Journal of Aeronautics* 26(3), 583-593.